Simultaneous polarization attraction and Raman amplification of a light beam in optical fibers

Philippe Morin, Stéphane Pitois, and Julien Fatome*

Laboratoire Interdisciplinaire Carnot de Bourgogne (ICB) UMR 6303 CNRS/Université de Bourgogne, 9 av. Alain Savary, 21078 Dijon, France
**Corresponding author: jfatome@u-bourgogne.fr*

Received March 20, 2012; revised June 5, 2012; accepted June 5, 2012;
posted June 6, 2012 (Doc. ID 165191); published July 18, 2012

In this paper, we demonstrate that it is possible to combine both Raman amplification and polarization attraction of a signal wave in a single optical fiber by means of a counterpropagating scheme. Experiments were performed near 1550 nm in a continuous wave regime and by means of a 10 Gbit/s return-to-zero signal injected in a 20 km-long low polarization mode dispersion optical fiber. Complete repolarization and 6.7 dB amplification of the signal wave was achieved by injecting a 850 mW, 1480 nm counterpropagating polarized pump wave. © 2012 Optical Society of America

OCIS codes: 060.0060, 060.4370, 190.4380, 190.5650, 250.4745.

1. INTRODUCTION

With the development of ultrahigh-bit-rate and transparent optical communication systems and their associated complex modulation formats and signal processing issues, several research groups have focused their attention on the conception of novel devices allowing a fast and all-optical control of the state of polarization (SOP) of a light beam. Indeed, in order to overcome electronic bottleneck and to go beyond the limit of current electronic feedback systems [1,2], nonlinear effects taking place in optical fibers have received much attention as a possible way to develop ultrafast polarization processing. For instance, Martinelli *et al.* have reported in [3,4] an original effect of polarization pulling in a fiber Raman amplifier based on polarization-dependent gain of the amplification process [3–10], whereas Thevenaz *et al.* have demonstrated in [11] that an all-optical polarization control can be obtained through stimulated Brillouin back-scattering occurring in optical fibers [11–17] Freitas *et al.* have also demonstrated that a polarization pulling process could be achieved thanks to a fiber-optical parametric amplifier [18]. Recently, it has also been reported that an all-optical polarization stabilization of a telecom signal can be achieved thanks to a counter propagating four-wave-mixing (FWM) process taking place in a low-birefringence, i.e., low polarization mode dispersion (PMD), optical fiber [19–22]. This nonlinear polarizer was experimentally observed by simultaneously injecting an arbitrary polarized signal wave and a polarized control pump beam via a counter propagating scheme. More precisely, we have shown in these previous works that, thanks to the FWM process, the pump wave induces a unidirectional exchange of energy between the orthogonal polarization components of the signal wave, thus leading to the so-called polarization attraction or "funnel" effect [23–30]. Here, an important feature of this phenomenon is that the polarization attraction process is supposed to act even though the pump and signal waves have different frequencies [29–31], basically because the FWM effect remains constantly phase-matched whatever the frequency detuning between the two waves [29–31].

Based on this last property, the aim of this work is thus to extend our preliminary work of [31] and to provide a proof-of-principle demonstrating that it is possible to combine both polarization attraction and Raman amplification in a unique segment of optical fiber thanks to a polarized frequency-shifted counter propagating optical pump wave. We would like to emphasize that the possibility of coupling these two fundamental optical functions in such a device has already been reported in a previous work, for which pioneering experiments were performed in the visible domain by means of kilowatt power nanosecond pulses injected in a few meters of isotropic optical fiber [31]. In this novel work, we focus our attention on the possibility to achieve such a process in the *C*-band around 1.55 μm, with both continuous waves and telecommunication signals, thus demonstrating the full potential of this device for practical applications. Section 2 of this manuscript is devoted to theoretical considerations dealing with Raman amplification and the polarization attraction process occurring in an optical fiber pumped by two counter propagating optical waves. In Section 3, we describe the experimental setup used to observe these two combined effects. Finally, Sections 4 and 5 are devoted to experimental results obtained either with a continuous optical signal or with a 10 Gbit/s Return-to-Zero (RZ) telecom signal, respectively.

2. THEORETICAL CONSIDERATIONS

Basically, the device presented in this paper and combining both Raman amplification and polarization stabilization is based on the nonlinear interaction between two counter propagating waves occurring in a kilometer-long low-PMD optical fiber (see Fig. 1).

For sake of simplicity and in order to catch the physics of the dual concept of the polarization attraction process combined with Raman amplification, we will consider in this theoretical part the case of a perfectly isotropic fiber. The case of

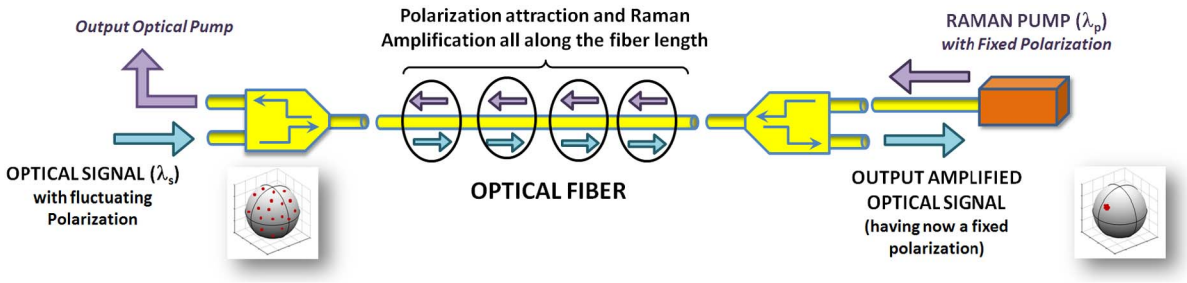

Fig. 1. (Color online) Principle of the device allowing both polarization attraction and Raman amplification.

standard kilometer-long optical fibers is a very complicated issue because of the random birefringence of this kind of fiber, which has been recently analyzed numerically and theoretically without Raman amplification by Kozlov *et al.* in [23] by means of averaging process or in [27] thanks to mathematical geometric tools. As the scope of the present manuscript is above all experimental, we will only introduce the concepts by means of the isotopic fiber case. To this aim, let us first consider two laser beams, a forward signal beam and a backward pump beam, that counter propagate with the same wavelength ($\lambda_s = \lambda_p$) in an isotropic optical fiber with arbitrary polarizations. The propagation of these two waves can be modeled by the following set of nonlinear coupled equations [29,30].

$$\frac{\partial u}{\partial t} + v_1 \frac{\partial u}{\partial z} = i\frac{2}{3}\gamma v_1[(|u|^2 + 2|v|^2)u + (2|\bar{u}|^2 + 2|\bar{v}|^2)u + 2\bar{u}\bar{v}^* v], \tag{1a}$$

$$\frac{\partial v}{\partial t} + v_1 \frac{\partial v}{\partial z} = i\frac{2}{3}\gamma v_1[(|v|^2 + 2|u|^2)v + (2|\bar{u}|^2 + 2|\bar{v}|^2)v + 2\bar{u}^*\bar{v}u], \tag{1b}$$

$$\frac{\partial \bar{u}}{\partial t} - v_2 \frac{\partial \bar{u}}{\partial z} = i\frac{2}{3}\gamma v_2[(|\bar{u}|^2 + 2|\bar{v}|^2)\bar{u} + (2|u|^2 + 2|v|^2)\bar{u} + 2uv^*\bar{v}], \tag{1c}$$

$$\frac{\partial \bar{v}}{\partial t} - v_2 \frac{\partial \bar{v}}{\partial z} = i\frac{2}{3}\gamma v_2[(|\bar{v}|^2 + 2|\bar{u}|^2)\bar{v} + (2|u|^2 + 2|v|^2)\bar{v} + 2u^* v\bar{u}], \tag{1d}$$

where u and v are the left and right circular polarizations of the signal beam, whereas $\bar{u}$ and $\bar{v}$ are the circular polarizations of the pump beam, respectively. γ is the usual nonlinear Kerr coefficient of the fiber, while v_1 and v_2 represent the group-velocities of the signal and pump waves, respectively. The first four terms on the right-hand side of each equation describe self-phase and cross-phase modulation effects. The last term describes the FWM process responsible for energy exchanges between the two circular polarization components of each wave. As demonstrated in previous works, this exchange of energy can lead to a polarization attraction effect providing that the pump wave is injected into the fiber with a circular polarization. In that case, the signal wave emerges from the fiber with a fixed circular polarization opposed to the pump, independently of its initial input SOP [29,30].

As seen from Eqs. (1), the nonlinear terms of the right-hand side are basically invariant with respect to a frequency shift of the backward wave, i.e., if $\bar{u}$ and $\bar{v}$ are changed into $\bar{u}e^{-i\Delta\omega t + i\Delta\beta z}$ and $\bar{v}e^{-i\Delta\omega t + i\Delta\beta z}$, respectively. In fact, as the frequency difference between the two waves increases ($\lambda_s > \lambda_p$), one should essentially modify these equations to include the Raman contribution to the Kerr nonlinearity. The resulting equations can thus be written as [31]

$$\begin{aligned}\frac{\partial u}{\partial t} + v_1\frac{\partial u}{\partial z} = i\gamma v_1\Bigg[&\left(\frac{2}{3}\alpha + \rho g_a(0)\right)|u|^2 + \left(\frac{4}{3}\alpha + \rho g_a(0) + \rho g_b(0)\right)|v|^2 \\ &+ \left(\frac{4}{3}\alpha + \rho g_a(0) + \rho g_a(\Omega)\right)|\bar{u}|^2 \\ &+ \left(\frac{4}{3}\alpha + \rho g_a(0) + \rho g_b(\Omega)\right)|\bar{v}|^2\Bigg]u \\ &+ i\gamma v_1\left[\left(\frac{4}{3}\alpha + \rho g_a(\Omega) + \rho g_b(0)\right)\right]\bar{u}v\bar{v}^*,\end{aligned} \tag{2a}$$

$$\begin{aligned}\frac{\partial v}{\partial t} + v_1\frac{\partial v}{\partial z} = i\gamma v_1\Bigg[&\left(\frac{2}{3}\alpha + \rho g_a(0)\right)|v|^2 + \left(\frac{4}{3}\alpha + \rho g_a(0) + \rho g_b(0)\right)|u|^2 \\ &+ \left(\frac{4}{3}\alpha + \rho g_a(0) + \rho g_a(\Omega)\right)|\bar{v}|^2 \\ &+ \left(\frac{4}{3}\alpha + \rho g_a(0) + \rho g_b(\Omega)\right)|\bar{u}|^2\Bigg]v \\ &+ i\gamma v_1\left[\left(\frac{4}{3}\alpha + \rho g_a(\Omega) + \rho g_b(0)\right)\right]\bar{v}u\bar{u}^*,\end{aligned} \tag{2b}$$

where γ is the nonlinear Kerr coefficient, ρ is the fractional Raman contribution to the total nonlinearity, $\alpha = (1 - \rho)$, and Ω is the pump-signal frequency detuning. Similar equations are obtained for the circular components of the pump wave simply by changing z into $-z$, u into $\bar{u}$ and v into $\bar{v}$. In these equations, g_a and g_b represent the Raman gains associated with co-rotating and counter rotating circularly polarized waves and are given by

$$g_a(\Omega) = \int_0^\infty \left(a(t)\exp(i\Omega t) + \frac{b(t)}{2}\exp(i\Omega t)\right)dt, \tag{3a}$$

$$g_b(\Omega) = \int_0^\infty b(t)\exp(i\Omega t)dt, \tag{3b}$$

where the two Raman response functions $a(t)$ and $b(t)$ can be approximated by [32]

$$a(t)+b(t)=\frac{\tau_1^2+\tau_2^2}{\tau_1\tau_2^2}\exp(-t/\tau_2)\sin(t/\tau_1), \tag{4a}$$

$$b(t)=\frac{2r}{\tau_2}\exp(-t/\tau_2). \tag{4b}$$

In these equations, $\tau_1 = 32$ fs, $\tau_2 = 12$ fs, and r represents the relative values of the parallel and orthogonal Raman gains in the linear basis components ($r \approx 0.2$).

Here, it is important to notice that, even if the configuration studied in the present work seems similar to one described in [7] and based on Raman induced nonlinear polarization rotation (NPR), the physical mechanism involved in the polarization attraction process is different. As shown by the last terms of Eqs. (1) and (2), the attraction phenomenon is based on a FWM interaction between the two circular components (right and left) of each counter propagative wave and not on a pulling process based on polarization depending gain (PDG) as in NPR systems [3,7]. Indeed, during the propagation in the polarization attractor, there is a constant and irreversible (because of the counter propagative configuration) exchange of energy between the two circular components of each wave. Consequently, as highlighted by the last terms of Eqs. (1) and (2), the efficiency of the FWM process is strongly dependent on both signal and pump powers, which involves working with close high powers for both counter propagative beams. This is not the case in NPR Raman systems, in which they can effectively consider a small signal wave, in which polarization is pulled by a counter propagating Raman pump beam thanks to NPR and PDG. Therefore, NPR systems need pump powers that are much above the one involved in the FWM approach and are very sensitive to residual relative intensity noise (RIN) because of the intrinsically PDG of the NPR process. Finally, a main feature of the FWM-based polarization attractor is that, as the global entropy of the system is conserved, all the disorder initially present in the incoming polarization signal vanishes from the system thanks to the pump, which is initially characterized by a well-defined fixed polarization state, and which comes out of the system with overall polarization fluctuations, which is not the case in NPR systems. Note that this last feature could be interesting to exploit so as to design an all-optical polarization scrambler.

In a previous study published in 2004 [31], we have demonstrated numerically from these equations and experimentally in the visible domain the possibility of combining Raman amplification and polarization attraction in the same optical fiber. In fact, it has been shown that the counter propagating polarized pump wave can act both as a polarization attractor and a source of energy for the signal wave. These pioneering experiments were conducted using a short piece of perfectly isotropic fiber with very high peak power nanosecond pulses whose wavelengths were in the visible domain, around 575 nm. In this paper, our approach is radically novel since we now consider a much longer standard optical fiber, having a low PMD, which allows the device to be compatible with continuous wave (cw), pulse train or telecom processing around 1.55 μm and involving average powers below 1 W. Even though the residual birefringence of such a fiber is very small, experimentally below 0.05 ps/km$^{1/2}$, it cannot rigorously be considered as perfectly isotropic. Nevertheless, it was shown in a recent work [20–24] that such a fiber can be seen as a concatenation of short individual polarization attractors for the signal wave, so that an effective polarization attraction effect can occur at the fiber output thanks to an average phenomenon. This basic approach was confirmed in [25–27]. In fact, one of the most important consequences is that the possibility to use such a long optical fiber results in a significant increase of the effective nonlinear interaction length between the counter propagating waves, thus involving beam powers compatible with telecom applications. Finally, it is also important to note that the counter propagating Raman amplification effect is fundamentally not affected by the presence of a weak fiber birefringence. As a consequence, one can expect that such a long low-PMD fiber pumped by an adequate counter propagating beam could act both as a polarization attractor and a Raman amplifier for the signal wave, thanks to an average process similar to that observed in [20,23]. In other words, we believe that our system can be considered as a succession of short individual polarization attractors in which the signal is simultaneously repolarized and amplified as described by Eqs. (2). This assumption will be confirmed through the experimental evidence reported in the section below.

3. EXPERIMENTAL SETUP

Figure 2 illustrates the experimental setup used to investigate the combined effects of Raman amplification and polarization attraction. At the transmitter side, pulses with full-width at half maximum (FWHM) of 2.5 ps and a repetition rate of 10 GHz are first generated using a mode-locked fiber laser (MLFL), operating at a wavelength of 1545 nm. The pulses are then broadened to 45 ps by an optical band pass filter (OBPF) and data encoded by means of an intensity Mach–Zehnder modulator (MZM) driven by a 10 Gb/s $2^7 - 1$ pseudorandom bit sequence (PRBS). A polarization scrambler is inserted to introduce random polarization fluctuations at a rate of 0.625 kHz. Before injection into the optical fiber, an erbium doped fiber amplifier (EDFA) was used to reach the suitable average power of 24 dBm (250 mW). The fiber under test is a 20 km long nonzero dispersion shifted fiber (NZDSF). The dispersion, dispersion slope, nonlinear coefficient, and PMD are 0.2 ps/nm/km, 0.09 ps/nm^2/km, 1.7 (W · km)$^{-1}$, and 0.03 ps/km$^{1/2}$, respectively. The crucial advantage of using kilometer-long standard optical fibers is that the polarization attraction process is no longer restricted to circular polarization states interaction and nanosecond, kilowatt experiments as in the isotropic case. Indeed, it was previously demonstrated that a fixed but arbitrary polarized counter propagating pump beam injected in a kilometer-long NZDSF fiber could act as a polarization attractor for any input polarization states with average powers compatible with Telecom applications [21–23]. The fiber is then inserted between two wavelength-division multiplexing (WDM) couplers so as to inject and monitor the signal wave. The counter propagating Raman pump beam, which allows us to control the polarization as well as to amplify the signal, was a fixed arbitrary polarized incoherent wave having a spectral bandwidth of 40 GHz centered around 1480 nm and with an average power that can be adjusted between 0 and 1 W. At the receiver, the SOP of the signal is analyzed onto the Poincaré sphere by means of a commercially available polarization analyzer. Finally, a 30 GHz bandwidth oscilloscope associated with a bit error rate (BER) analyzer allowed us to monitor in

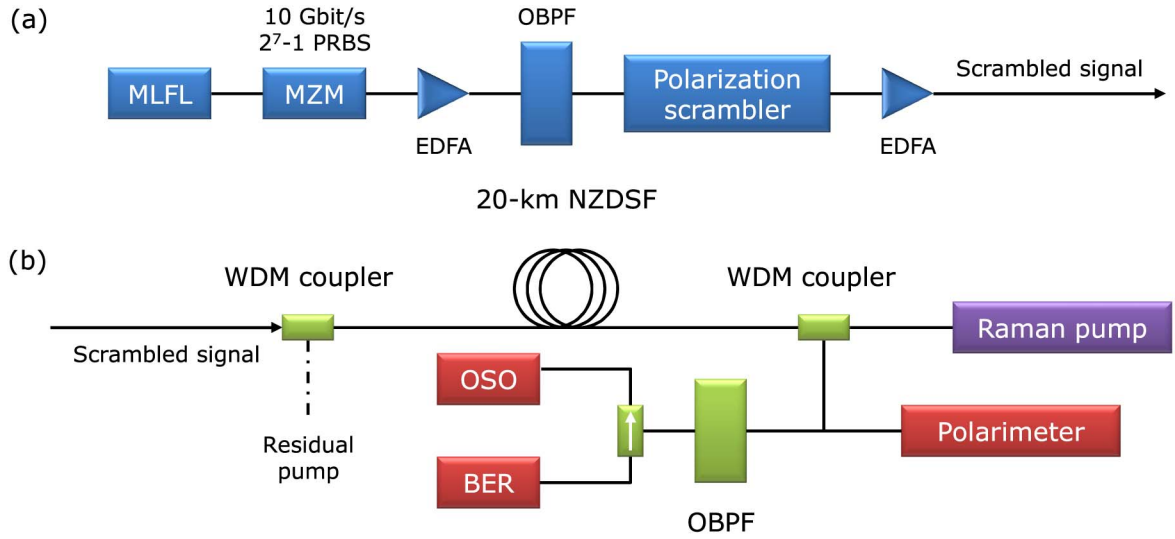

Fig. 2. (Color online) Experimental setup: (a) 10 Gb/s RZ transmitter; (b) all-optical polarization attraction block. MLFL, mode-locked fiber laser; MZM, Mach–Zehnder modulator.

real-time the intensity profile of the outcoming pulses and transmission quality.

4. EXPERIMENTAL RESULTS: CONTINUOUS OPTICAL SIGNAL

Experimental evidences of the combined effects of polarization attraction and Raman amplification were first achieved in the cw regime at 1548 nm. The SOP of the signal wave was measured at the output of the fiber as a function of the Raman pump power, for a fixed signal power of 250 mW. Results are shown in Fig. 3 for different pump powers ranging from 0 to 850 mW. In absence of Raman pump [Fig. 3(a)], and due to the initial polarization scrambling, the different points, representing the signal polarization states, are uniformly distributed onto the Poincaré sphere. As can be seen in Figs. 3(b)–3(d), when the pump power is gradually increased from 0 to 850 mW, all the signal polarizations asymptotically converge towards the same output SOP thanks to the polarization attraction effect [Fig. 3(d)]. Simultaneously, a signal intensity on/off gain of 6.7 dB was measured at the output of the fiber for a pump power of 850 mW, thanks to the counter propagating Raman amplification effect. Note that the maximum achievable on/off gain is certainly limited by the effect of Raman pump depletion due to the high initial signal power involved in the polarization attraction process. On the other hand, it is important to note that the pump power involved in the present experiments to achieve an efficient polarization attraction process is higher than previous results reported at 10 Gbit/s without Raman gain [21]. This phenomenon is also attributed to the Raman pump depletion effect.

Further information can be obtained by monitoring the output signal wave in the temporal domain thanks to a low-bandwidth oscilloscope. A linear polarizer was inserted just before the photodiode in order to simulate a polarization-dependent component, i.e., so that all polarization fluctuations are turned into intensity fluctuations. The oscilloscope was used in persistence mode to superimpose the different waveforms. The results are shown in Fig. 4 for a signal power fixed to 250 mW, without [Fig. 4(a)] and with [Fig. 4(b)] the 850 mW counter propagating Raman pump wave. When the pump wave is turned off [Fig. 4(a)], the temporal trace shows different levels of intensity, resulting from the different states of polarization induced by the initial polarization scrambling. When the pump wave is turned on [Fig. 4(b)], the initial power fluctuations induced by the polarization scrambling are significantly reduced, leading to a unique level of intensity at the output of the system and thus demonstrating the ability of our system to reduce polarization fluctuations without any polarization-dependent losses (PDL). Note that the vertical scale of Fig. 4 is the same for both recordings. Simply, an additional variable attenuator was inserted in the case of Fig. 4(b) so as to counteract the Raman gain.

5. EXPERIMENTAL RESULTS: 10 Gbit/s OPTICAL SIGNAL

In this section, and in order to underline the practical compatibility of our device with telecommunication applications, we

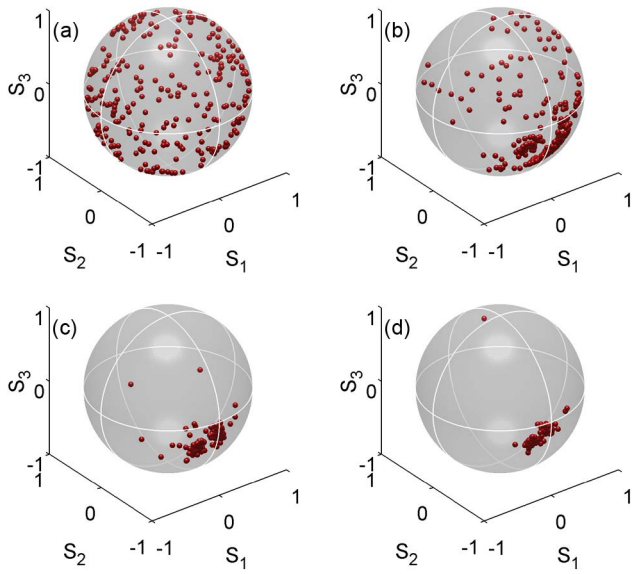

Fig. 3. (Color online) Evolution of the SOP of the output cw signal as a function of the Raman pump power. (a) 0 mW; (b) 340 mW; (c) 680 mW, and (d) 850 mW. The signal power was fixed to 250 mW.

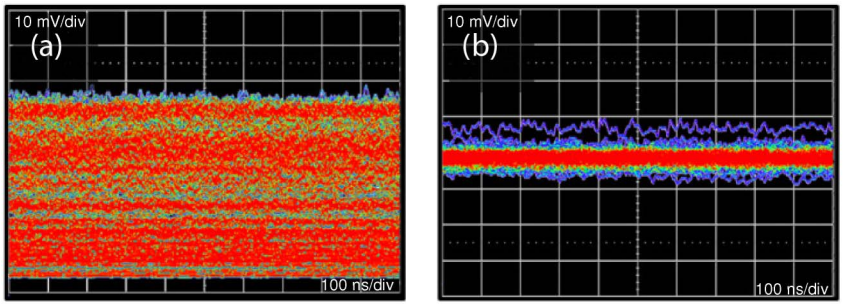

Fig. 4. (Color online) Intensity profile (detected behind a polarizer) of the output CW signal, without (a) and with (b) the 850 mW counterpropagating Raman pump wave. The signal power at the input of the fiber was fixed to 250 mW.

have replaced the initial cw by a 10 Gbit/s PRBS signal wave at 1545 nm. Let us recall that thanks to the counter propagating configuration of the system, both the polarization attraction and the Raman amplification effects are only sensitive to the average intensity profiles of the signal and pump waves, rather than on the short scale intensity profiles. In fact, the main issue that should be considered when using picosecond pulse trains is the temporal broadening induced by the group-velocity dispersion of the fiber and Kerr nonlinearity. Nevertheless, with the fiber parameters used in our experiment, the excess of temporal broadening observed after propagation in the optical fiber is kept below 10 ps. Figure 5 shows on the Poincaré sphere the SOP of the 10 Gb/s signal at the output of the system as a function of the pump power and for a fixed signal power of 24 dBm (250 mW). As can be seen, all signal polarizations asymptotically converged towards the same output SOP when pump power was increased from 0 mW [Fig. 5(a)], 200 mW [Fig. 5(b)], 400 mW [Fig. 5(c)], and, finally, 850 mW [Fig. 5(d)]. Note that an on/off Raman gain of 6.7 dB was simultaneously achieved when pump power was increased up to 850 mW.

The efficiency of the polarization attraction process can be also evaluated by calculating the degree of polarization (DOP) of the output signal polarization. The DOP is defined as

$$\mathrm{DOP} = \frac{\sqrt{\langle S_1^2\rangle + \langle S_2^2\rangle + \langle S_3^2\rangle}}{S_0},$$

where S_i are the Stokes parameters of the signal and $\langle\,\rangle$ denotes an averaging process over 256 initial conditions and evaluated on a time scale much longer than the duration of the input polarization fluctuations. The DOP permits us to measure the spread of output polarization fluctuations on the Poincaré sphere and thus to quantify the efficiency of the attraction phenomenon. In fact, low values of the DOP indicate that polarization scrambling leads to large temporal fluctuations of the SOP all over the Poincaré sphere, whereas a DOP value close to unity is associated with a nearly constant and stabilized output SOP. Figure 6 shows the evolution of the output signal DOP as a function of Raman pump power. The DOP of the signal, which has initially low value, close to 0.4, increases strongly when the counter propagating Raman pump is injected into the fiber so as to reach a value very close to unity for a Raman pump power above 600 mW. A maximum value of 0.98 was achieved for a pump power of 850 mW. It is also important to note that since the effect of polarization attraction is based on an FWM interaction, the efficiency of the process depends on both signal and pump powers. Consequently, decreasing the signal power with a constant pump power will dramatically affect the efficiency of the phenomenon in the same way as a variation of pump power depicted in Fig. 6.

The efficiency of the polarization attraction process is more striking when directly monitored in the temporal domain. The

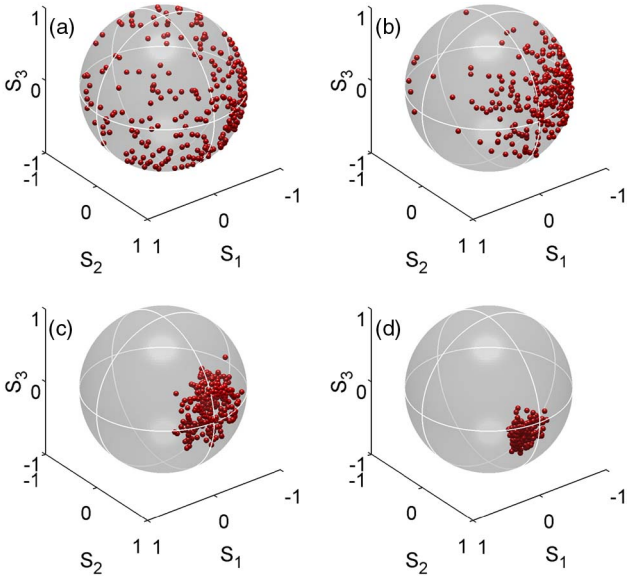

Fig. 5. (Color online) Evolution of the SOP of the 10 Gbit/s signal wave at the output of the fiber as a function of Raman pump power. (a) 0 mW; (b) 200 mW; (c) 400 mW, and (d) 850 mW. The signal power was fixed to 24 dBm. A 6.7 dB on/off gain was achieved for a pump power of 850 mW.

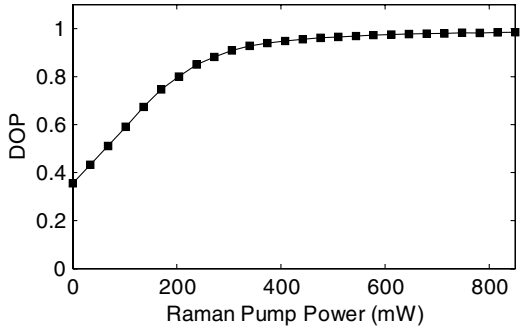

Fig. 6. Evolution of the DOP of the 10 Gbit/s signal wave at the output of the fiber as a function of Raman pump power. The signal power was fixed to 250 mW, whereas the Raman pump power varies from 0 to 850 mW.

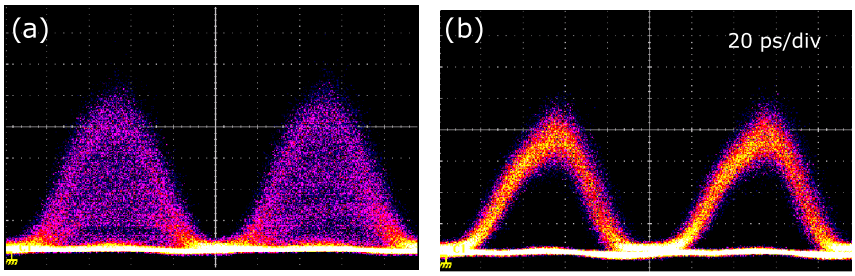

Fig. 7. (Color online) Eye-diagram (detected behind a polarizer) of the output 10 Gbit/s, without (a) and with (b) the counterpropagating Raman pump wave. Signal and pump average power were fixed to 24 dBm (250 mW) and 850 mW, respectively.

10 Gbit/s eye-diagrams were recorded through a linear polarizer so as to transfer the whole polarization fluctuations directly into the time domain. Resulting eye-diagrams are represented in Fig. 6 in absence [Fig. 6(a)] and in presence of the counter propagating Raman pump wave [Fig. 6(b)]. In the pump-free configuration, the initial polarization fluctuations induced by the polarization scrambler are transformed into intensity variations after the polarizer, leading to a complete closure of the eye-diagram [Fig. 6(a)]. On the contrary, when the 850 mW pump beam is injected into the fiber, thanks to the polarization attraction process, all the output pulses emerge from the fiber with the same SOP. As a result, the initial intensity fluctuations linked to the polarization variations are greatly reduced, leading to a significant opening of the eye-diagram [Fig. 6(b)] and recovering of the data. At the same time, the Raman amplification process leads to an intensity gain of the signal beam of nearly 6.7 dB. These results clearly demonstrate the ability of our system to combine simultaneously an all-optical control and stabilization of the polarization state as well as an amplification of a 10 Gbit/s RZ telecom signal.

Finally, we have also measured the corresponding BER of the 10 Gbit/s signal as a function of the average power incoming on the receiver (Fig. 8). The reference is illustrated by the back-to-back configuration (i.e., at the fiber input) in circles. At the output of the system, when the polarization of the signal is scrambled, corresponding to the close eye-diagram of Fig. 6(a), the BER is limited to 3.10^{-3} (triangles). When the 850 mW counter propagating pump wave is injected at the opposite side of the fiber (squares), the quality of the transmission is greatly improved. Indeed, data are completely recovered behind the polarizer, allowing error-free transmission with low BER penalties on the receiver compared to back-to-back measurements (circles). More precisely, a power penalty of 1 dB is achieved at a BER of 10^{-9} as well as a weak amount of RIN in the eye-diagram, which is mainly attributed to the combined effect of chromatic dispersion and nonlinear impairments occurring during the propagation as well as the degradation of the signal-to-noise ratio due to Raman amplification but not to Raman PDG. Indeed, as the polarization attractor is based on FWM, it does not introduce any additional Raman PDG and one has to introduce an additional polarizer in order to transfer all polarization fluctuations into the time domain so as to characterize the related RIN into the eye-diagram. This is very dramatic in the NPR approach, in particular for nonlinear post-processing, since all PDG variations are directly transferred into the intensity profile, such as a nonlinear polarizer [7]. These weak intensity fluctuations, observed in the eye-diagram of Fig. 7(b), could also be attributed to residual polarization fluctuations that are not completely vanished from the system thanks to the pump [not a single point onto the output Poincaré sphere in Fig. 5(d)]. But, it is important to notice that these intensity fluctuations are still present without initial polarization scrambling, which proves that they originate from propagation impairments and not from the polarization stabilization process.

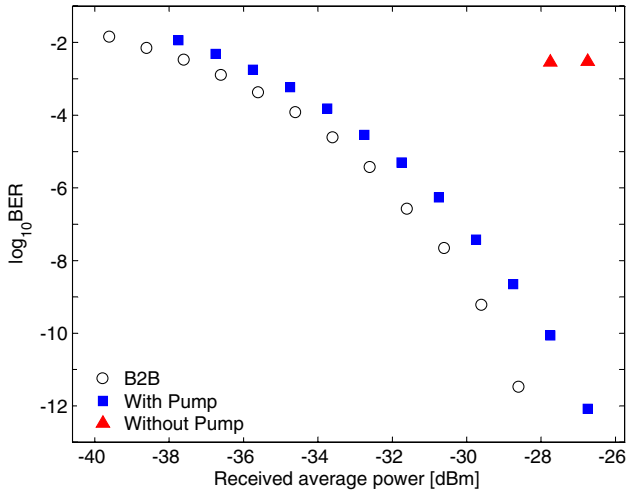

Fig. 8. (Color online) Evolution of the BER as a function of average power in back-to-back configuration (circles); at the output of the system, with polarization scrambling and after a polarizer with (squares) and without (triangles) the 850 mW counterpropagating pump beam.

6. CONCLUSION

In this paper, we report an all-optical device that allows combining both polarization attraction and amplification of an optical signal in a unique segment of standard optical fiber. The polarization attraction phenomenon is based on an FWM process, whereas the optical amplification is obtained thanks to stimulated Raman scattering. These two effects were obtained simultaneously in the telecom domain by injecting a polarized counter propagating pump wave in the optical fiber with a wavelength around 1480 nm. The experimental results were performed with both a continuous signal wave and a 10 Gbit/s PRBS RZ optical signal around 1550 nm.

ACKNOWLEDGMENTS

This work was supported by the European Research Council (ERC) starting grant PETAL project and by the Conseil Régional de Bourgogne.

REFERENCES

1. M. Martinelli, P. Martelli, and S. M. Pietralunga, "Polarization stabilization in optical communications systems," J. Lightwave Technol. **24**, 4172–4183 (2006).
2. B. Koch, R. Noé, V. Mirvoda, H. Griesser, S. Bayer, and H. Wernz, "Record 59 krad/s polarization tracking in 112 Gb/s 640 km PDM-RZ-DQPSK transmission," Photon. Technol. Lett. **22**, 1407–1409 (2010).
3. M. Martinelli, M. Cirigliano, M. Ferrario, L. Marazzi, and P. Martelli, "Evidence of Raman-induced polarization pulling," Opt. Express **17**, 947–955 (2009).
4. M. Ferrario, V. Gilardone, P. Martelli, L. Marazzi, and M. Martinelli, "Effective all-optical polarization control induced by Raman nonlinear amplification," in *European Conference and Exhibition on Optical Communication (ECOC'2010)* (IEEE, 2010), paper P1.19.
5. V. V. Kozlov, J. Nuño, J. D. Ania-Castañón, and S. Wabnitz, "Theory of fiber optic Raman polarizers," Opt. Lett. **35**, 3970–3972 (2010).
6. V. V. Kozlov, J. Nuño, J. D. Ania-Castañón, and S. Wabnitz, "Theoretical study of optical fiber Raman polarizers with counterpropagating beams," J. Lightwave Technol. **29**, 341–347 (2011).
7. F. Chiarello, L. Ursini, L. Palmieri, and M. Santagiustina, "Polarization attraction in counterpropagating fiber Raman amplifiers," Photon. Technol. Lett. **23**, 1457–1459 (2011).
8. L. Ursini, M. Santagiustina, and L. Palmieri, "Raman nonlinear polarization pulling in the pump depleted regime in randomly birefringent fibers," Photon. Technol. Lett. **23**, 254–256 (2011).
9. N. J. Muga, M. F. S. Ferreira, and A. N. Pinto, "Broadband polarization pulling using Raman amplification," Opt. Express **19**, 18707–18712 (2011).
10. S. V. Sergeyev, "Activated polarization pulling and de-correlation of signal and pump states of polarization in a fiber Raman amplifier," Opt. Express **19**, 24268–24279 (2011).
11. L. Thevenaz, A. Zadok, A. Eyal, and M. Tur, "All-optical polarization control through Brillouin amplification," in *Optical Fiber Communication Conference*, Technical Digest (CD) (Optical Society of America, 2008), paper OML7.
12. A. Zadok, E. Zilka, A. Eyal, L. Thévenaz, and M. Tur, "Vector analysis of stimulated Brillouin scattering amplification in standard single-mode fibers," Opt. Express **16**, 21692–21707 (2008).
13. J. Fatome, S. Pitois, and G. Millot, "Experimental evidence of Brillouin-induced polarization wheeling in highly birefringent optical fibers," Opt. Express **17**, 12612–12618 (2009).
14. Z. Shmilovitch, N. Primerov, A. Zadok, A. Eyal, S. Chin, L. Thevenaz, and M. Tur, "Dual-pump push-pull polarization control using stimulated Brillouin scattering," Opt. Express **19**, 25873–25880 (2011).
15. A. Galtarossa, L. Palmieri, M. Santagiustina, L. Schenato, and L. Ursini, "Polarized Brillouin amplification in randomly birefringent and unidirectionally spun fibers," Photon. Technol. Lett. **20**, 1420–1422 (2008).
16. M. Sagues and A. Loayssa, "Orthogonally polarized optical single sideband modulation for microwave photonics processing using stimulated Brillouin scattering," Opt. Express **18**, 22906–22914 (2010).
17. A. Zadok, A. Eyal, and M. Tur, "Stimulated Brillouin scattering slow light in optical fibers," Appl. Opt. **50**, E38–E49 (2011).
18. J. F. L. Freitas, C. J. S. de Matos, M. B. Costa e Silva, and A. S. L. Gomes, "Impact of phase modulation and parametric gain on signal polarization in an anomalously dispersive optical fiber," J. Opt. Soc. Am. B **24**, 1469–1474 (2007).
19. S. Pitois, J. Fatome, and G. Millot, "Polarization attraction using counter-propagating waves in optical fiber at telecommunication wavelengths," Opt. Express **16**, 6646–6651 (2008).
20. J. Fatome, S. Pitois, P. Morin, and G. Millot, "Observation of light-by-light polarization control and stabilization in optical fibre for telecommunication applications," Opt. Express **18**, 15311–15317 (2010).
21. J. Fatome, P. Morin, S. Pitois, and G. Millot, "Light-by-light polarization control of 10 Gb/s RZ and NRZ telecommunication signals," J. Sel. Top. Quantum Electron. **18**, 621–628 (2012).
22. P. Morin, J. Fatome, C. Finot, S. Pitois, R. Claveau, and G. Millot, "All-optical nonlinear processing of both polarization state and intensity profile for 40 Gbit/s regeneration applications," Opt. Express **19**, 17158–17166 (2011).
23. V. V. Kozlov, J. Nuno, and S. Wabnitz, "Theory of lossless polarization attraction in telecommunication fibers," J. Opt. Soc. Am. B **28**, 100–108 (2011).
24. V. V. Kozlov and S. Wabnitz, "Theoretical study of polarization attraction in high birefringence and spun fibers," Opt. Lett. **35**, 3949–3951 (2010).
25. E. Assémat, S. Lagrange, A. Picozzi, H. R. Jauslin, and D. Sugny, "Complete nonlinear polarization control in an optical fiber system," Opt. Lett. **35**, 2025–2027 (2010).
26. E. Assémat, D. Dargent, A. Picozzi, H. R. Jauslin, and D. Sugny, "Polarization control in spun and telecommunication optical fibers," Opt. Lett. **36**, 4038–4040 (2011).
27. E. Assémat, A. Picozzi, H. R. Jauslin, and D. Sugny, "Hamiltonian tools for the analysis of optical polarization control," J. Opt. Soc. Am. B **29**, 559–571 (2012).
28. V. V. Kozlov, K. Turitsyn, and S. Wabnitz, "Nonlinear repolarization in optical fibers: polarization attraction with copropagating beams," Opt. Lett. **36**, 4050–4052 (2011).
29. S. Pitois, G. Millot, and S. Wabnitz, "Nonlinear polarization dynamics of counterpropagating waves in an isotropic optical fiber: theory and experiments," J. Opt. Soc. Am. B **18**, 432–443 (2001).
30. S. Pitois, A. Picozzi, G. Millot, H. R. Jauslin, and M. Haelterman, "Polarization and modal attractors in conservative counterpropagating four-wave interaction," Europhys. Lett. **70**, 88–94 (2005).
31. S. Pitois, A. Sauter, and G. Millot, "Simultaneous achievement of polarization attraction and Raman amplification in isotropic optical fibers," Opt. Lett. **29**, 599–601 (2004).
32. S. Trillo and S. Wabnitz, "Parametric and Raman amplification in birefringent fibers," J. Opt. Soc. Am. B **9**, 1061–1082 (1992).